Adenine Radicals in the Gas Phase: An Experimental and Computational Study of Hydrogen Atom Adducts to Adenine

Xiaohong Chen,[†] Erik A. Syrstad,[†] Minh Tho Nguyen,[‡] Pascal Gerbaux,*[,§] and František Tureček*[,†]

Department of Chemistry, Bagley Hall, Box 351700, University of Washington, Seattle, Washington 98195-1700, Department of Chemistry, University of Leuven, B-3001 Leuven, Belgium, and Department of Organic Chemistry, University of Mons-Hainaut, Mons, Belgium

Received: June 3, 2005; In Final Form: July 20, 2005

The elusive hydrogen atom adduct to the N-1 position in adenine, which is thought to be the initial intermediate of chemical damage, was specifically generated in the gas phase and characterized by neutralization−reionization mass spectrometry. The N-1 adduct, 1,2-dihydroaden-2-yl radical (**1**), was generated by femtosecond electron transfer to N-1-protonated adenine that was selectively produced by electrospray ionization of adenine in aqueous-methanol solution. Radical **1** is an intrinsically stable species in the gas phase that undergoes specific loss of the N-1-hydrogen atom to form adenine, but does not isomerize to the more stable C-2 adduct, 1,2-dihydroaden-1-yl radical (**5**). Radicals **1** that are formed in the fifth and higher electronically excited states of $\Delta E \geq 2.5$ eV can also undergo ring-cleavage dissociations resulting in expulsion of HCN. The relative stabilities, dissociation, and transition state energies for several hydrogen atom adducts to adenine have been established computationally at highly correlated levels of theory. Transition state theory calculations of 298 K rate constants in the gas phase, including quantum tunnel corrections, indicate the branching ratios for H-atom additions to C-8, C-2, N-3, N-1, and N-7 positions in adenine as 0.68, 0.20, 0.08, 0.03, and 0.01, respectively. The relative free energies of adenine radicals in aqueous solution point to the C-8 adduct as the most stable tautomer, which is predicted to be the predominating (>99.9%) product at thermal equilibrium in solution at 298 K.

Introduction

Nucleobase residues in nucleic acids are the target of high-energy particles and reactive species in the complex process of DNA damage.[1] Among the several chemical pathways of DNA damage, protonation of nucleobase anion−radicals produced by electron capture (the so-called direct mechanism)[2] and addition of hydrogen atoms produced by radiolysis of water (indirect mechanism, Scheme 1)[3] result in the formation of nucleobase radicals, as shown for adenine and its derivatives (R = H, CH_3, 1′-ribosyl, etc.), that can undergo further degradation reactions.

Although both the direct and indirect mechanism can produce hydrogen atom adducts to adenine, the structures of these reactive intermediates can differ due to the different chemistries involved. While radiolysis of adenine-containing nucleosides has been studied in solution,[4] crystals,[5] and frozen glasses,[6] the chemical nature of hydrogen atom adducts to adenine and their reactivity in propagating chemical damage have not been fully elucidated. The radiolysis data seem to point to the initial formation of an H-atom adduct to the N-1 position in adenine by protonation of an adenine anion−radical.[4f] The initially formed N-1-H adducts are thought to isomerize to C-8 [4f] or C-5 adducts,[6b,c] as inferred from electron paramagnetic resonance (EPR) spectra. However, EPR measurements of transient species in the condensed phase face the problem that it is difficult to distinguish the radicals of interest among many other open-shell radiolytic products produced by an inherently nonselective process.

SCHEME 1

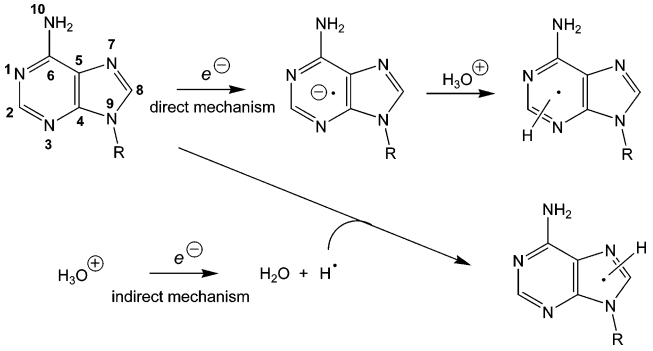

To study reactive transient species, it is advantageous to resort to the rarefied gas phase where one can avoid effects of solvent and environment and investigate the *intrinsic properties* of the molecules or radicals of interest. We have shown previously for several heterocyclic systems,[7] including the RNA nucleobase uracil,[8] that hydrogen atom adducts can be generated specifically in the gas phase by femtosecond collisional electron transfer to gas-phase cations that have been prepared by the methods of ion chemistry. The ion chemistry methods that we developed relied either on selective protonation of basic sites in the nucleobase[9] or well-defined dissociations of suitable precursor cation−radicals that were prepared by charge-exchange ionization and thus produced the desired cations under conditions of

[†] University of Washington.
[‡] University of Leuven.
[§] University of Mons-Hainaut.

10.1021/jp0529725 CCC: $30.25
Published on Web 08/18/2005

internal energy control.[8b] The radicals produced from the cations by collisional electron transfer are investigated by neutralization−reionization mass spectrometry (NRMS),[10] whereby the undissociated radicals and their dissociation products are nonselectively ionized, and the ions are separated by mass, detected, and quantified. The NRMS approach provides virtually complete product analysis and, when combined with laser photoexcitation[11] and variable-time methods,[12] it also yields information on the electronic states and unimolecular dissociation kinetics of transient species.

In the present paper we address the problem of specific generation of hydrogen atom adducts to adenine and study their properties by mass spectrometric methods that are complemented by high-level quantum chemical calculations. We wish to show that by using a combination of electrospray and gas-phase ionization with stable isotope labeling one can obtain kinetic data that characterize the chemistry and energetics of adenine radicals in the gas phase.

Experimental Section

Materials. Adenine (99% pure) was purchased from Sigma-Aldrich and used as received. D_2O (99.9% D), acetic acid-d_4 (99.5% D), acetone-d_6 (99.9% D), and methanol-d_4 (99.8% D), all Cambridge Isotope Laboratories, and methanol (Fisher) were used for synthetic work as received. The solvents used for electrospray ionization were distilled in Pyrex and kept in sodium-free vessels to minimize contamination with alkali metal ions.

[*N-9-*^{2}*H,N-10-*^{2}*H*$_2$]*adenine* was prepared by H/D exchange of the labile protons in adenine as follows. Adenine (32 mg) was sonicated to dissolve in 1.0 mL of D_2O. The solvent was evaporated in vacuo and the solid was used for measurements.

[*8-*^{2}*H*$_1$]*Adenine.* Adenine (1 g) was dissolved in 30 mL of warm D_2O (60−70 °C) containing two drops of acetic acid-d_4. The solution was stirred overnight, the solvents were evaporated to dryness in vacuo, and the procedure was repeated twice. A 20-mg aliquot of the solid product was dissolved in 2 mL of methanol and the solvent was evaporated in vacuo. Mass spectrum (direct probe, 140 °C): *m/z* 136 ($M^{+\bullet}$). The deuterium position was assigned from the ^{1}H NMR spectrum (DMSO-d_6, 25 °C) that showed a singlet at δ 8.087.[13]

Measurements. Neutralization−reionization mass spectra were measured on the University of Washington (UW) tandem quadrupole acceleration−deceleration mass spectrometer[14] that was equipped with a special electrospray ion source[15] providing 1−2 nA currents of the desired ions in the high-vacuum region. Adenine solutions at 50−100 μM in 70/30 methanol−water were electrosprayed and the ions were transmitted by an electrodynamic ion funnel[16] at 0.5−0.7 Torr into the vacuum system. The ions were further transmitted by a radio frequency-only octopole (10^{-3} Torr, 70 V bias) to a differentially pumped region (10^{-4} Torr) and focused by a wide-open quadrupole mass filter (55−60 V bias) onto an acceleration lens (−7150 V). The 7200 eV ions were discharged by collisions with dimethyl disulfide that was admitted to the vacuum system at pressures to achieve 70% transmittance of the precursor ion beam. Residual ions were reflected by a special electrostatic lens and the neutral products were allowed to drift to a reionization cell where they were reionized by collisions with molecular oxygen at 70% beam transmittance. The ions were decelerated to 70−75 eV and mass analyzed by a second quadrupole mass analyzer that was scanned at unit mass resolution. Typically, 100−200 scans were collected and averaged to provide the spectra presented here. Another set of neutralization−reionization mass spectra was measured at 8 keV on the University of Mons large-scale six-sector tandem mass spectrometer as described previously.[17] Ions were prepared by chemical ionization (CI) of gaseous adenine with $(CH_3)_2COH^+$/acetone or $(CD_3)_2COD^+$/acetone-d_6 at 200 °C, selected by mass, and neutralized by collisions with Xe at 70% ion beam transmittance. Oxygen was used for reionization at 70% beam transmittance. The spectra were obtained as kinetic energy scans.

Calculations. Standard ab initio and density functional theory calculations were performed using the Gaussian 98[18a] and Gaussian 03 suite of programs.[18b] Geometries were optimized with the hybrid functional (B3LYP)[19] and the 6-31+G(d,p) basis. Spin unrestricted calculations (UB3LYP and UMP2) were used for open-shell systems. In the UB3LYP calculations, $\langle S^2 \rangle$ operator expectation values ranged from 0.751 to 0.767 for doublet states. Contamination by higher spin states in UMP2 calculations was treated by a standard annihilation procedure.[20] Optimized structures were characterized by harmonic frequencies as local minima (all real frequencies) and saddle points (one imaginary frequency). The calculated frequencies (scaled by 0.963) and moments of inertia were used to calculate 298 K enthalpies and entropies using the rigid rotor−harmonic oscillator approximation. The optimized geometries are available as Tables S1−S17 and Figures S1 and S2 (Supporting Information), and the harmonic frequencies can be obtained from the corresponding author upon request. Dissociation pathways were studied by changing one internal coordinate in 0.025−0.1 Å steps while fully optimizing the other internal coordinates. Improved energies for potential energy surface mapping were obtained by single-point calculations that combined B3LYP and spin-projected MP2 energies calculated with the 6-311++G(2d,p) basis set, according to eq 1.

$$E(\text{B3-PMP2}) = 0.5[E(\text{B3LYP}) + E(\text{PMP2})] \qquad (1)$$

These calculations, which are denoted as B3-PMP2,[21] have been shown previously by us[22] and others[23] to provide improved accuracy for several closed-shell and open-shell systems of medium (10−50 atoms) size. Further expansion of the basis set by adding shells of d and f functions on carbon and nitrogen atoms and including two shells of p functions on hydrogens, 6-311++G(3df,2p), resulted in B3-PMP2 relative energies that were very similar (within ±3 kJ mol^{-1} root-mean-square deviation) to those calculated with B3-PMP2/6-311++G(2d,p). This is consistent with our previous study of basis set effects in an aromatic system.[22c] For selected systems, we carried out coupled cluster[24] single-point energy calculations with single, double, and perturbational triple excitations, CCSD(T),[25] using the 6-31G(d,p) basis set. These were extrapolated to the larger basis sets in the usual fashion.[26] The obtained energies are referred to as effective CCSD(T)/basis set. Excited-state energies were calculated using time-dependent density functional theory[27] with B3LYP/6-311++G(2d,p).

Solvation free energies were calculated by B3LYP/6-31+G(d,p) using both the original polarizable continuum model (PCM)[28a] included in Gaussian 98 and the refined model[28b] included in Gaussian 03. Structures were reoptimized by PCM-B3LYP/6-31+G(d,p) using standard parameters (water dielectric constant, atomic, and van der Waals radii) included in Gaussian 98 and 03.

Unimolecular rate constants were calculated by the Rice−Ramsperger−Kassel−Marcus (RRKM) theory using Hase's program[29] that was recompiled for Windows XP.[30] The RRKM rate constants were obtained by direct count of quantum states at internal energies that were increased in 2 kJ mol^{-1} steps from

TABLE 1: Proton Transfer Energies for the Reaction (Adenine + H)$^+$ + H_2O → Adenine + H_3O^+

ion	ΔH_{298}(g)[a]	ΔG_{298}(g)[b]	ΔG_{298}(aq)[c,d]	pK_a[e]
1$^+$	251	243	55.5 (29.2)	8.0 (3.4)[d] (4.2)[f]
2$^+$	243	235	46.0 (17.0)	6.3 (1.2)[d]
3$^+$	216	211	41.9 (14.9)	5.6 (0.9)[d]
4$^+$	162	158	−22.1 (−39.9)	−5.6 (−8.7)[d]

[a] Gas-phase reaction enthalpies from CCSD(T)/6-311++G(3df,2p) energies, B3LYP/6-31+G(d,p) zero point vibrational energies, and 298 K molar enthalpies. [b] Gas-phase reaction free energies. [c] Reaction free energies in water including PCM-B3LYP/6-31+G(d,p) solvation free energies for adenine, **1**$^+$, **2**$^+$, **3**$^+$, and **4**$^+$, and experimental solvation free energies for H_3O^+ and water (ref 28b). [d] The values in parentheses used solvation energies calculated by the original Polarizable Continuum Model (ref 28a). [e] Calculated for infinite dilution in 55.51 M water. [f] Experimental value from ref 38.

the transition state up to 400 kJ mol^{-1} above the reactant. Rotations were treated adiabatically, and the calculated $k(E,J,K)$ microscopic rate constants were Boltzmann-averaged over the thermal distribution of rotational states at 298 K, corresponding to the ion source temperature, to provide canonical rate constants $k(E)$.

Transition state theory (TST) calculations of thermal rate constants were performed using the standard TST formula.[31] The requisite rotational and vibrational partition functions for reactants and transition states were obtained from B3LYP/6-31+G(d,p) harmonic frequencies and moments of inertia using the rigid rotor−harmonic oscillator model.

Tunnel corrections were performed as described previously.[32] Briefly, B3-PMP2/6-311++G(2d,p) potential energy profiles were calculated at 15−20 points along the relevant reaction coordinates[33] and corrected for zero-point vibrational energies in the $3N - 7$ normal modes transversal to the reaction coordinate.[34] The corrected potential energy profiles (Figures S3−S9, Supporting Information) were fitted with Eckart functions of the same height,[35] such as to least-squares match the width at all points of the barrier. The Eckart fits were quite tight and showed <1.2% root-mean-square deviation from the B3-PMP2/6-311++G(2d,p) barrier widths. Barrier permeabilities ($G(E)$) were calculated for the fitted Eckart barriers using the standard formula[36] and convoluted with Boltzmann distribution functions (eq 2) to obtain tunnel correction coefficients ($\kappa(T)$). The latter were used to correct the TST rate constants ($k_{TST}(T)$), according to eq 3.[36]

$$\kappa(T) = e^{E_{TS}/kT} \int_{E_0}^{\infty} G(E) e^{-E/kT} dE \quad (2)$$

$$k_{corr}(T) = \kappa(T) k_{TST}(T) \quad (3)$$

Results and Discussion

Ion Preparation. Our strategy for the preparation of adenine radicals relies on first forming precursor ions by selective protonation, followed by neutralization by femtosecond collisional electron transfer. Thus, the hydrogen atom is introduced in the adenine molecule in two steps but in an opposite order than in the direct mechanism of DNA damage where the proton follows the electron. Adenine is known to be selectively protonated at N-1 in aqueous solution[37] with a pK_a for deprotonation equal to 4.2.[38] This is consistent with our calculations of topical pK_a values,[9b,39] which show that N-1 is 48−130 times more basic than N-3, which is the second most basic center in adenine (Table 1). The N-7 and NH_2 (labeled as N-10, Scheme 1) positions are even less basic (Table 1). Hence, protonation by electrospray that occurs in acidic solvent

CHART 1

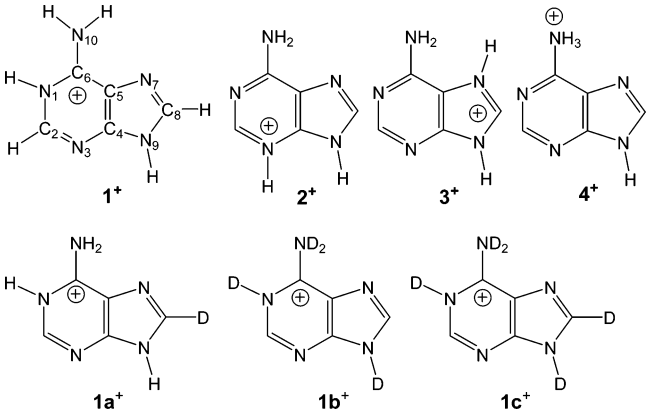

microdroplets[40] is expected to be highly selective (∼97% at 298 K) by producing N-1-protonated adenine cations **1**$^+$ (Chart 1). It should be noted that N-1 is also the most basic site in adenine gas-phase clusters with one and two molecules of water.[39] Thus, prototropic isomerization of ions **1**$^+$ in solution, in solvent clusters during transfer to the gas phase, and in isolated ions is endoergic, so that structure **1**$^+$ is always favored under equilibrium conditions. Unimolecular isomerizations of gas-phase **1**$^+$ by proton migration forming tautomers protonated at C-2 (**5**$^+$), N-3 (**2**$^+$), and N-10 (**4**$^+$) were calculated to require activation energies of 285, 272, and 191 kJ mol^{-1} which are inaccessible to ions produced by electrospray.[41] A firm conclusion from this analysis is that adenine ions sampled for collisional neutralization have structure **1**$^+$. We note that protonation at N-1 was also considered to occur in fast-atom bombardment ionization from a glycerol matrix, and the ions thus formed were assigned structure **1**$^+$.[42]

Electrospray was also used to generate deuterium-labeled ions **1a**$^+$ (C-8-D), **1b**$^+$ (N-1-D, N-9-D, ND_2), and **1c**$^+$ (N-1-D, C-8-D, N-9-D, ND_2) (Chart 1). Note that the exchangeable protons in adenine (H-9 and NH_2) are equilibrated with those of the solvent and cannot be labeled selectively in solution. The gas-phase ions produced by electrospray undergo a large number of collisions with solvent and residual gas molecules during transport from atmospheric pressure to the high-vacuum system. It is therefore reasonable to assume that the adenine ions that are subjected to collisional electron transfer are rotationally and vibrationally thermalized at the ambient temperature (293−298 K).[41] We note that electrospray ionization of adenine produced **1**$^+$ as the predominating (>97%) ion species that was accompanied by only a small fraction (<3%) of a sodium ion adduct, as reported previously.[15] No solvent clusters or proton-bound dimers were observed in the electrospray ionization mass spectra, in keeping with the theoretical analysis of thermodynamic stabilities of such species.[39]

In contrast to electrospray ionization, gas-phase protonation of adenine depends on the topical proton affinities (PA) of the basic centers, N-1, N-3, N-7, N-9, and the NH_2 group, which have been calculated by effective CCSD(T)/6-311++G(3df,2p) as 939, 932, 904, 746, and 850 kJ mol^{-1}, respectively.[9b] The topical PA indicate that it is practically impossible to selectively protonate the N-1 position in the gas phase under the usual conditions of chemical ionization without protonating N-3 and N-7. Hence, gas-phase protonation of adenine, even if carried out under mild conditions using gas-phase acids such as NH_4^+ (PA(NH_3) = 853 kJ mol^{-1}) and $(CH_3)_2COH^+$ (PA(acetone) = 812 kJ mol^{-1})[43] is expected to yield mixtures of ions **1**$^+$, **2**$^+$, and **3**$^+$. The proportions of these ions depend on the experimental conditions. Proton transfer in the gas phase is known to

CHART 2

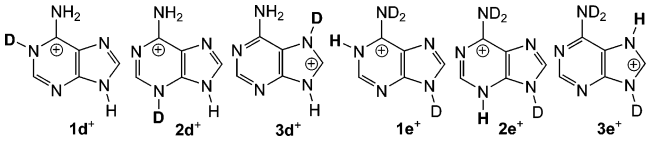

occur at the collisional frequency for reactions that have $\Delta G°_T < -40$ kJ mol^{-1}.[44] Hence, under kinetic control $\mathbf{1}^+$, $\mathbf{2}^+$, and $\mathbf{3}^+$ should be formed in equimolar (0.33) fractions. However, because protonated adenine can react with neutral adenine molecules that are present at large excess in the ion source, the less stable ions $\mathbf{2}^+$ and $\mathbf{3}^+$ can be depleted to form the most stable tautomer $\mathbf{1}^+$. Under equilibrium conditions at the ion source temperature (473 K), we calculate the relative $\Delta G°_{473}$ for $\mathbf{1}^+$, $\mathbf{2}^+$, and $\mathbf{3}^+$ as 0.0, 7.5, and 30.6 kJ mol^{-1}, respectively, leading to the respective equilibrium molar fractions equal to 0.87, 0.13, and <0.01. The kinetically controlled and equilibrium molar ratios represent the two extremes of ion populations for $\mathbf{1}^+$, $\mathbf{2}^+$, and $\mathbf{3}^+$. We show later that dissociations of radicals **1**, **2**, and **3** shed some light on the precursor ion populations.

Gas-phase protonation has the advantage of allowing one to selectively introduce isotope labels into adenine ions. Gas-phase deuteronation with $(CD_3)_2COD^+$ occurs without H/D exchange at N-9 and in the NH_2 group, producing a mixture of ions $\mathbf{1d}^+$, $\mathbf{2d}^+$, and $\mathbf{3d}^+$ (Chart 2). Likewise, protonation with $(CH_3)_2COH^+$ of [N_9-D, ND_2]-adenine yields a mixture of $\mathbf{1e}^+$, $\mathbf{2e}^+$, and $\mathbf{3e}^+$ that was used to make the corresponding D-labeled radicals.

The N-10-protonated tautomer $\mathbf{4}^+$ is inaccessible by direct protonation of the adenine amino group in the gas phase or solution. We attempted to generate ion $\mathbf{4}^+$ by an ion−molecule reaction of 6-chloropurine cation−radical with ammonia, which produced a $C_5H_6N_5^+$ ion in a yield sufficient for a NRMS study. However, upon collisional activation this ion showed dissociations that were indistinguishable from those of ions generated by gas-phase protonation of adenine. The identity of the putative ion $\mathbf{4}^+$ will be addressed later in the paper. The structures and dissociations of protonated adenine tautomers and cation−radicals have been reported recently[9b,39] and will not be discussed here in detail.

Adenine Radicals. $^+NR^+$ of $\mathbf{1}^+$ gave rise to the spectrum shown in Figure 1. This shows a substantial survivor ion of $\mathbf{1}^+$ at *m*/*z* 136, which attests to the stability of the intermediate radical **1** on the 5.9 μs time scale of the experiment. Major dissociation products are adenine, which is detected as its cation−radical at *m*/*z* 135, and a number of smaller fragments (Figure 1a). Most of these (*m*/*z* 108, 81, 66, 65, 54, 53, 43−38, and 28−26) can be assigned to post-reionization dissociations of [adenine]$^{+\bullet}$. This is corroborated by the electron ionization[45] and $^+NR^+$ mass spectra of adenine that show the same major fragments, although $^+NR^+$ clearly results in more extensive dissociation (Figure 1b and inset). $^+NR^+$ of $\mathbf{1}^+$ produces another fragment at *m*/*z* 91, which is very weak in the $^+NR^+$ mass spectrum of [adenine]$^{+\bullet}$ and absent in the CAD spectrum of $\mathbf{1}^+$, and thus must be formed by dissociation of radical **1** by combined or consecutive losses of H, HCN, and NH_3 which indicate a ring cleavage.

$^+NR^+$ of $\mathbf{1a}^+$ shows specific (>95%) elimination of light hydrogen, indicating that the C-8-H hydrogen atom does not participate in the dissociation (Figure 2a). $^+NR^+$ of $\mathbf{1b}^+$ results in loss of mostly D, although minor loss of H and consecutive losses of (H + D) are also observed (Figure 2b). $^+NR^+$ of $\mathbf{1c}^+$ shows exclusive loss of D (Figure 2c), indicating that the hydrogen atom at C-2 is involved neither in direct dissociation, nor in migration to other positions that would result in its loss.

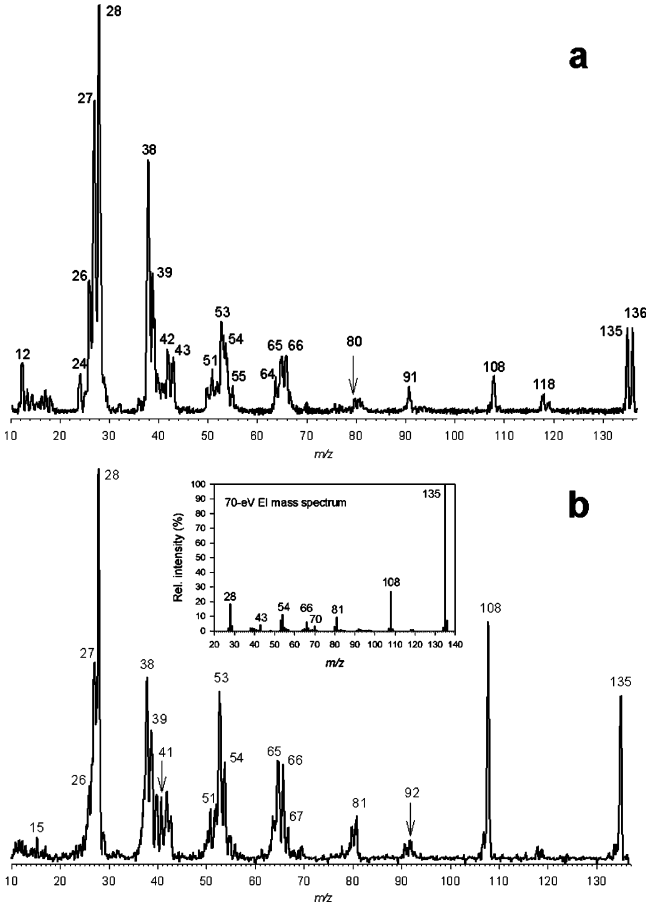

Figure 1. Neutralization (CH_3SSCH_3, 70% transmittance)−reionization (O_2, 70% transmittance) mass spectra of (a) $\mathbf{1}^+$ by electrospray ionization and (b) [adenine]$^{+\bullet}$ by 70-eV electron ionization. The inset shows the 70-eV electron ionization mass spectrum of adenine.

Noteworthy are the isotope effects on the loss of H/D that affect the relative intensities of the survivor ions, denoted as [M + H,D], and [adenine]$^{+\bullet}$, denoted as [M], such that the [M + H,D]/[M] intensity ratios are measured as 0.92, 1.32, 1.50, and 2.12 for $\mathbf{1}^+$, $\mathbf{1a}^+$, $\mathbf{1b}^+$, and $\mathbf{1c}^+$, respectively. A comparison of the $^+NR^+$ and collision-induced dissociations (CID) of $\mathbf{1a}^+$ and $\mathbf{1b}^+$ shows major differences in the product distributions in that CID results in much less regiospecific H/D loss, which occurs nearly statistically regardless of the original label position.[9b]

$^+NR^+$ mass spectra of the ions generated by gas-phase protonation or ion−molecule reactions are shown in Figure 3. The spectrum of the mixture of protonated adenines $\mathbf{1}^+$−$\mathbf{3}^+$ (Figure 3a) is indistinguishable from that of the supposed ion $\mathbf{4}^+$ (Figure 3b). Because radicals **1**−**3** and **4** are expected to dissociate differently, the similar behavior upon $^+NR^+$ of their precursor ions indicates that the latter are in fact composed of the same mixture of isomers. This can be explained by ion $\mathbf{4}^+$ undergoing exothermic prototropic isomerization to the more stable isomers $\mathbf{1}^+$−$\mathbf{3}^+$, which is most likely mediated by ammonia in the ion source, according to eqs 4 and 5 for conversion to $\mathbf{1}^+$ and analogously for conversions to $\mathbf{2}^+$ and $\mathbf{3}^+$.

$$\mathbf{4}^+ + NH_3 \rightarrow \text{adenine} + NH_4^+ \qquad \Delta G_{298}(g) = -5.5 \text{ kJ mol}^{-1} \quad (4)$$

$$NH_4^+ + \text{adenine} \rightarrow NH_3 + \mathbf{1}^+ \qquad \Delta G_{298}(g) = -79.5 \text{ kJ mol}^{-1} \quad (5)$$

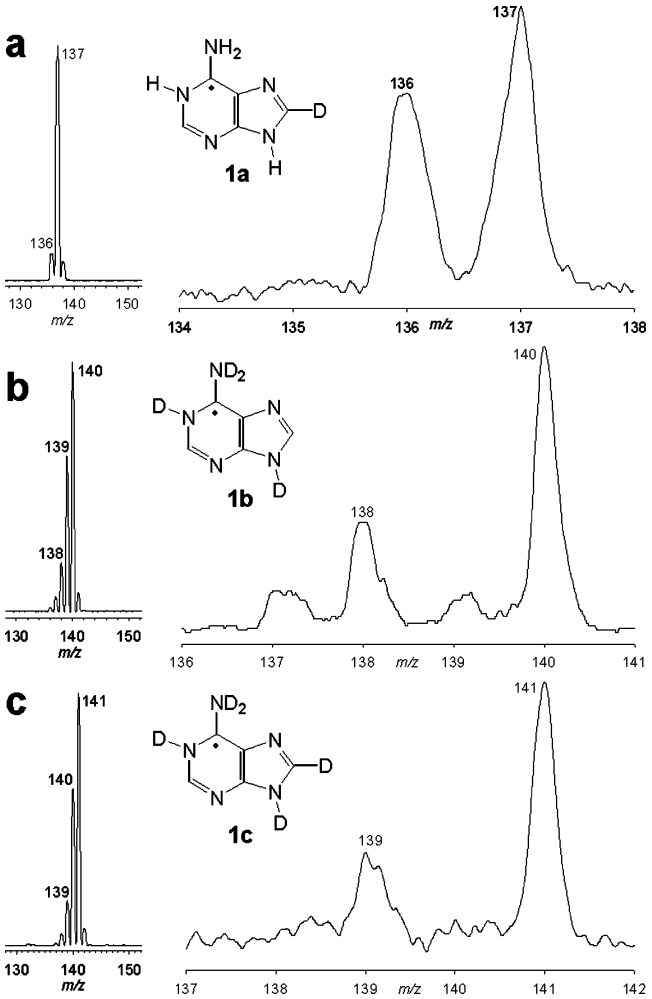

Figure 2. Neutralization (CH_3SSCH_3, 70% transmittance)−reionization (O_2, 70% transmittance) mass spectra of (a) $\mathbf{1a}^+$, (b) $\mathbf{1b}^+$, and (c) $\mathbf{1c}^+$. The insets show the $(M + H,D)^+$ regions in the ESI mass spectra.

The isomerization may involve an ion−dipole complex of NH_4^+ and adenine, but this mechanistic detail was not studied here.

A conspicuous feature of the $^+NR^+$ mass spectra in Figure 3a,b is the low relative abundance of the survivor ions. After deconvoluting the incompletely resolved peaks at *m*/*z* 136, denoted as [M + H], and *m*/*z* 135, denoted as [M], we obtain an [M + H]/[M] ratio of 0.14 to be compared with 0.92 for $\mathbf{1}^+$ (see above). Other differences between the $^+NR^+$ mass spectra in Figure 1a and Figure 3a,b are due to different neutralization reagents used, different scan modes, and peak overlap due to low mass resolution in the kinetic energy scans in Figure 3a,b.

$^+NR^+$ of $\mathbf{1d}^+$−$\mathbf{3d}^+$ gives well-defined survivor ions at *m*/*z* 137 (Figure 4a), with an [M + H,D]/[M] intensity ratio of 0.54. Radicals **1d**−**3d** lose D and H in a 2.3:1 ratio. $^+NR^+$ of $\mathbf{1e}^+$−$\mathbf{3e}^+$ gives survivor ions at *m*/*z* 139, with an [M + H,D]/[M] intensity ratio of 0.39 (Figure 4b). Radicals **1e**−**3e** lose mainly H, with an H/D ratio of 5:1. The combined elimination of (H, HCN + NH_3) shows a specific loss of D from **1d**−**3d** (*m*/*z* 91, Figure 4a) and retention of one D from **1e**−**3e** (*m*/*z* 92, Figure 4b).

In summarizing this part, collisional neutralization of protonated adenine tautomers forms fractions of stable radicals corresponding to hydrogen atom adducts to adenine. The main dissociation of these radicals is loss of a hydrogen atom. The mechanisms for radical dissociations will be discussed in the following section.

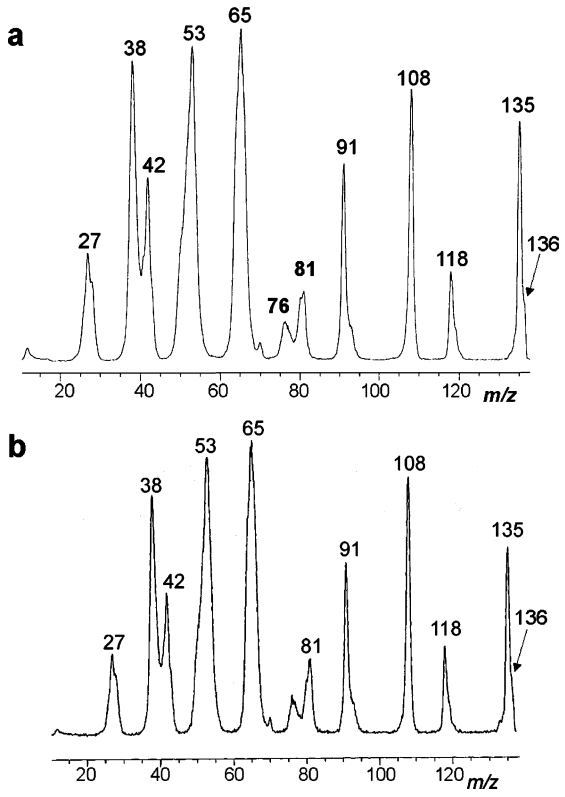

Figure 3. Neutralization (Xe, 70% transmittance)−reionization (O_2, 70% transmittance) mass spectra of (a) $\mathbf{1}^+$−$\mathbf{3}^+$ by gas-phase protonation of adenine with $(CH_3)_2C-OH^+$, and (b) by ion−molecule reaction of $[6\text{-chloropurine}]^{+\bullet}$ with ammonia.

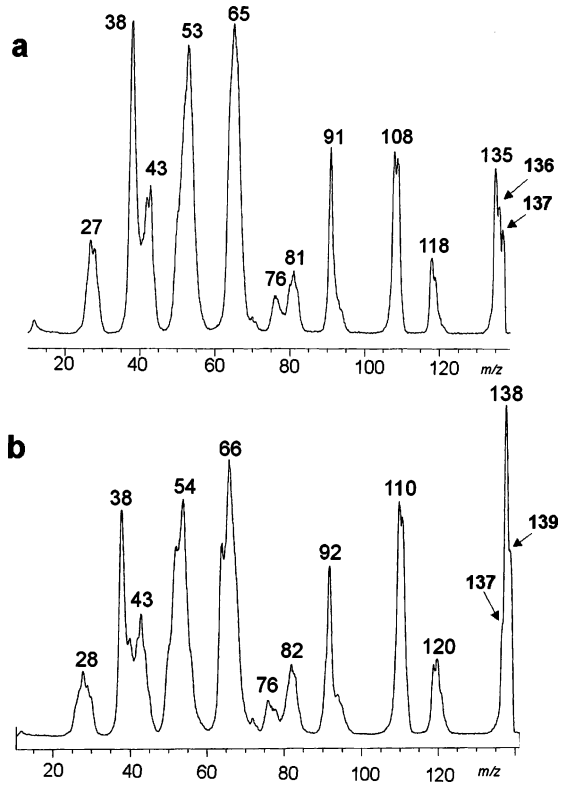

Figure 4. Neutralization (Xe, 70% transmittance)−reionization (O_2, 70% transmittance) mass spectra of (a) $\mathbf{1d}^+$−$\mathbf{3d}^+$ by gas-phase deuteronation of adenine with $(CD_3)_2C-OD^+$ and (b) $\mathbf{1e}^+$−$\mathbf{3e}^+$ by gas-phase protonation of [N_9-D, ND_2]adenine with $(CH_3)_2C-OH^+$.

Radical Structures and Energetics. To aid the interpretation of radical dissociations upon $^+NR^+$ we obtained optimized

TABLE 2: Relative Energies of Adenine Radicals

		relative energy[a]					
		6-311++G(2d,p)		6-311++G(3df,2p)			
radical		B3-PMP2	CCSD(T)[b]	B3-PMP2	CCSD(T)[b]		$\Delta G°_{298}$(aq)[c]
1	(N-1-H)	60	56	56	51	52[d]	36
2	(N-3-H)	63	65	58	58	61	34
3	(N-7-H)	58	59	54	54	57	42
4	(N-10-H)	*e*					
5	(C-2-H)	33	31	33	31	33	29
6	(C-4-H)	95	86	95	84	87	73
7	(C-5-H)	71	64	71	63	67	58
8	(C-6-H)	88	79	90	82	81	*f*
9	(C-8-H)	0	0	0	0	0	0

[a] Relative enthalpies in kJ mol^{-1} including B3LYP/6-31+G(d,p) zero-point vibrational energies and referring to 0 K. [b] Effective energies from basis set expansions: E[CCSD(T)/large basis set] = E[CCSD(T)/6-31G(d,p)] + E[PMP2/large basis set] − E[PMP2/6-31G(d,p)]. [c] Relative free energies in the polar dielectric (water) at 298 K. [d] Relative free energies in the gas phase at 298 K. [e] Radical **4** is not a bound structure. [f] PCM calculation of the solvation free energy of radical **8** failed.

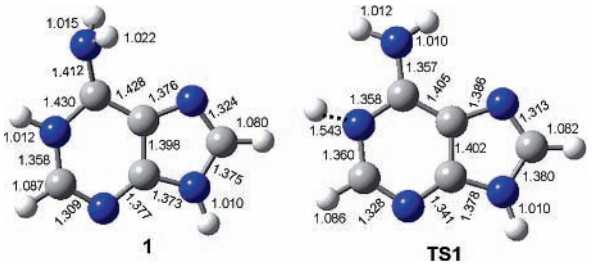

Figure 5. B3LYP/6-31+G(d,p) optimized structures of **1** and **TS1**. Bond lengths in angstroms.

CHART 3

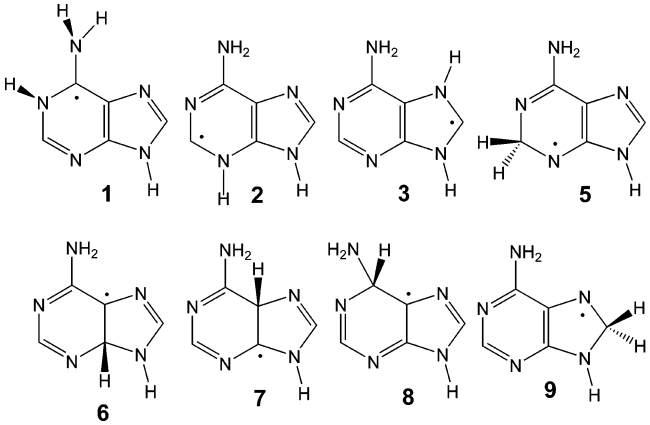

geometries and relative, dissociation, and transition state energies for [adenine + H]$^{\bullet}$ tautomers **1**−**9** (Chart 3). Radicals **1**−**3** and **5**−**9** are local energy minima. In contrast, the N-10-H adduct (**4**) was found not to be a local energy minimum, and upon attempted optimization it dissociated by N-10−H bond cleavage. The optimized structure of radical **1** (Figure 5) shows it to have an out-of-plane NH_2 group due to a combined pyramidization at C-6 and rotation about the N-10−C-6 bond. The N-1−H-1 bond is also out of the ring plane due to pyramidization at N-1. Compared with **1**, the precursor ion $\mathbf{1}^+$ is planar and shows different lengths for the N-1−C-6 and N-10−C-6 bonds.[9b,39] Vertical neutralization of $\mathbf{1}^+$ thus results in excitation of several stretching and deformation vibrational modes in **1**, which combined result in deposition of 70 kJ mol^{-1} internal energy through Franck−Condon effects. The optimized structures of **2**, **3**, and **5**−**9** are given in the Supporting Information (Figures S1 and S2).

Table 2 shows that the C-8-H adduct **9** is the most stable of adenine radicals, followed by the C-2-H adduct **5**. The N-1-H (**1**), N-3-H (**2**), and N-7-H (**3**) adducts are comparably stable but are 51−58 kJ mol^{-1} destabilized against **9**. The C-4-H (**6**), C-5-H (**7**), and C-6-H (**8**) adducts are 84, 63, and 82 kJ mol^{-1} less stable than **9**. We note that relative stabilities of selected adenine radicals have also been calculated recently by DFT methods in connection with a pulse radiolysis study.[46]

Of interest were also transition state structures and energies for dissociations and isomerizations of **1**−**9**. Dissociation of the N-1−H-1 bond in **1** proceeds through **TS1**, in which the departing H_1 increases the out-of plane tilt, while the NH_2 group rotates to become nearly aligned with the ring plane (Figure 5). The reaction path for the N-1−H-1 dissociation in **1** is depicted in Figure 6a. The B3LYP potential energy surface shows a transition state (**TS1**) that occurs at 1.543 Å, but is followed by a false minimum at d(N-1- - -H) ∼ 2.4 Å. The B3-PMP2 fit shows a more realistic PES, which monotonically descends from **TS1** (at 1.452 Å) to the products. Similar effects were observed for calculations of reaction paths for N-3−H-3 bond dissociation in **2** and N-7−H-7 bond dissociation in **3**. The optimized geometries of **2** and **3** and the potential energy surfaces for their N−H bond dissociations are given as Supporting Information (Figures S3−S9).

The competing dissociation of the N-10−H-10a bond in **1** is shown in Figure 6b. The B3LYP/6-31+G(d,p) potential energy shows a profile that monotonically increases with N−H separation, while the B3-PMP2 fit shows a regular transition state at d(N-10- - -H) = 1.737 Å. The relative energies for dissociations of **1**, as calculated at four levels of theory, are summarized in Table 3 and the structures are arrayed in a potential energy diagram (Figure 7). This shows that loss of H-1 through **TS1**, forming adenine, is the energetically most favorable pathway. Loss of H-10 through **TS2**, forming adenine imine tautomer **11**, competes with N-1−C-2 bond dissociation (**TS3**) forming the open-ring intermediate **10**. However, a further dissociation of **10** by loss of HCN, forming 5-formamidylimidazol-4-yl radical (**12**), requires a high threshold energy, indicating that **10** is a kinetic cul-de-sac intermediate. Likewise, cleavage of the imidazole ring in **1** and expulsion of an HCN molecule containing N-7 and C-8 to form the 4-amino-6-imino-3,6(*3H*)-dihydropyrimid-5-yl radical (**13**) is a highly endothermic dissociation that can hardly at all compete with the N-1−H-1 bond dissociation on the same potential energy surface.

The dissociations of the N-3-H adduct **2** show features similar to those of **1** (Figure 8). Dissociation of the N-3−H bond follows the minimum energy reaction path that proceeds through **TS4** to form adenine. Dissociation of the N-10−H bond in **2** has a relatively high threshold energy forming the imine tautomer **14**

TABLE 3: Transition State Energies for Dissociations of 1−3 and 5−9

			transition state energy[a]			
			6-311++G(2d,p)		6-311++G(3df,2p)	
reactant	TS[b]	products	B3-PMP2	CCSD(T)[c]	B3-PMP2	CCSD(T)[c]
1	**TS1**	adenine + H	81	94	82	97
	TS2	**11** + H	108	119	109	121
	TS3	10	117	118	121	125
		12 + HCN[d]	207	193	216	209
		13 + HCN[d]	228	212	240	233
2	**TS4**	adenine + H	77	86	79	89
	TS5	**14** + H	183	180	185	183
	TS6		146	144	151	153
		15 + HCN[d]	219	208	229	226
		16 + HCN[d]	192	178	203	197
3	**TS7**	adenine + H	87	94	88	95
	TS8	**9**	142	145	143	146
5	**TS9**	adenine + H	101	113	99	111
6	**TS10**	adenine + H	62	78	60	76
7	**TS11**	adenine + H	73	87	71	84
8	**TS12**	adenine + H	71	90	68	87
9	**TS13**	adenine + H	130	138	128	135

[a] In units of kJ mol^{-1}, including B3LYP/6-31+G(d,p) zero-point corrections. [b] For transition state geometries from B3-PMP2/6-311++G(2d,p) fits of potential energy surfaces. [c] Effective energies from basis set expansion: E[CCSD(T)/large basis set] ≈ E[CCSD(T)/6-31G(d,p)] + E[PMP2/large basis set] − E(PMP2/6-31G(d,p)]. [d] Energies at 0 K thermochemical thresholds.

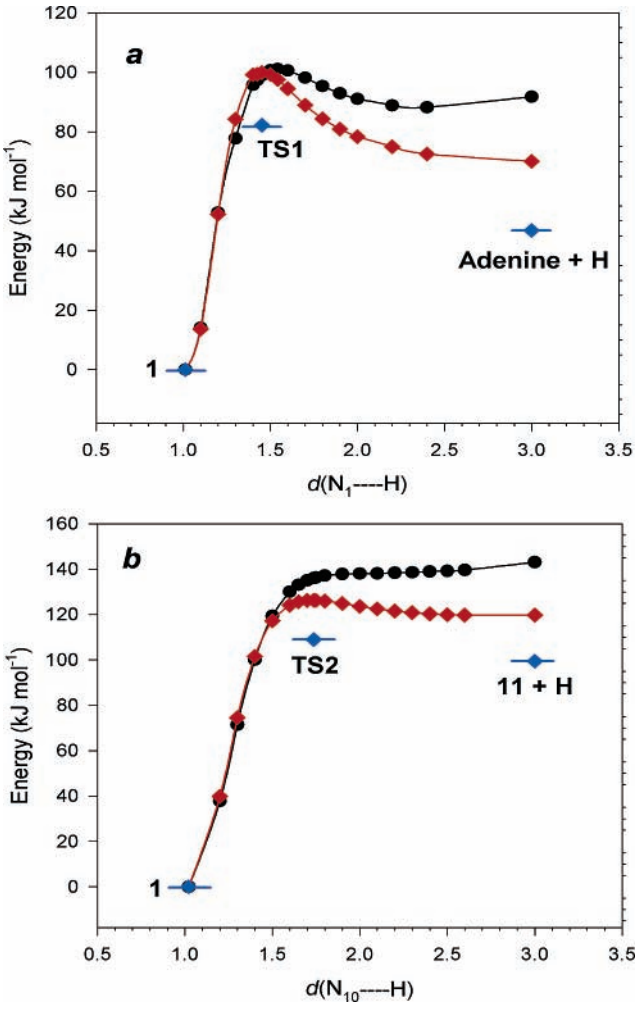

Figure 6. Potential energy profiles for N−H bond dissociations in **1**. (a) Dissociation of the N_1−H bond. (b) Dissociation of the N_{10}−H bond.

and requires >180 kJ mol^{-1} in **TS5**. The high energy for the N-10−H bond dissociation favors the competing cleavage of the C-8−N-9 bond through **TS6** leading to loss of HCN and formation of the 4-imino-6-amino-3,4-dihydro-(3*H*)pyrimid-5-yl radical (**15**) (Figure 8). The alternative cleavage of the pyrimidine ring in **2** followed by loss of HCN forming the 4-imino-5-aminomethylideneimidazolyl radical **16** requires a yet higher threshold energy and therefore may not be competitive with the loss of the hydrogen atom.

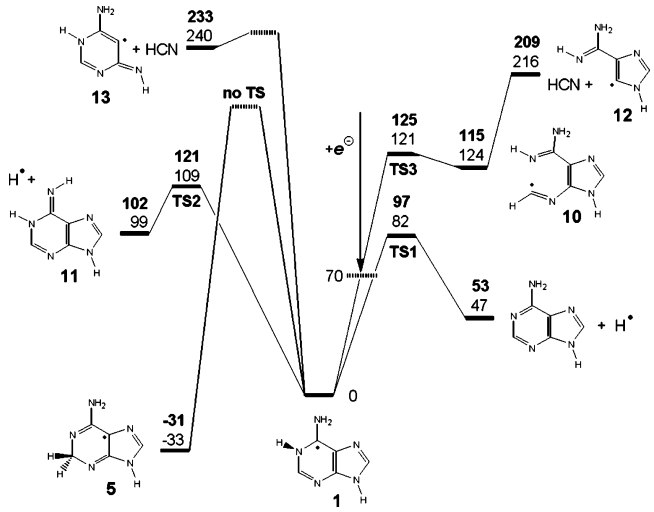

Figure 7. Potential energy profile for dissociations and isomerizations of **1** at the ground doublet electronic state. Light face numerals: B3-PMP2/6-311++G(3df,2p) calculations with ZPVE corrections. Bold numerals: Effective CCSD(T)/6-311++G(3df,2p) calculations with ZPVE corrections.

Dissociations by loss of H from radicals **3** and **5**−**9** were also investigated by reaction path mapping with B3-PMP2/6-311++G(2d,p), and the relevant TS energies from calculations at four levels of theory are summarized in Table 3. The reaction paths are given as Supporting Information (Figures S3−S9).

To aid the interpretation of the deuterium labeling experiments, we also investigated the reaction paths for isomerizations by H-atom 1,2-migrations in **1** and **3**. The latter radical shows a regular transition state (**TS8**) for 1,2-H-atom migration from N-7 to C-8 at 143 kJ mol^{-1} above **3** and 197 kJ mol^{-1} above **9**. Note that **TS8** is a saddle point that breaks through the high-energy PES region that separates the valleys for H-atom loss from **3** and **9** that lead up to transition states of much lower energies (88 and 128 kJ mol^{-1} for **TS7** and **TS13**, respectively,

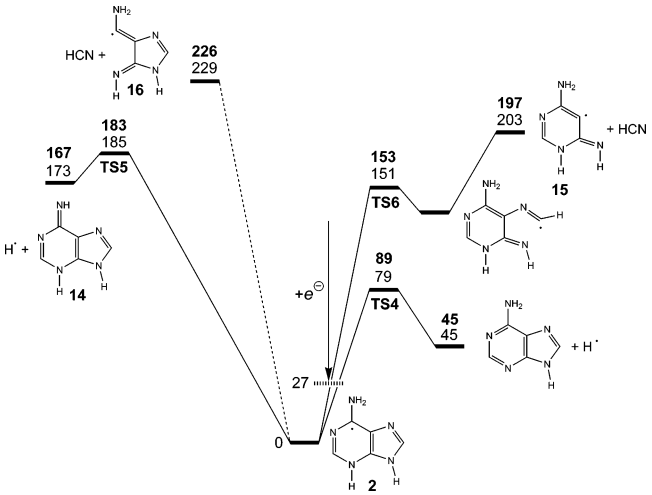

Figure 8. Potential energy profile for dissociations and isomerizations of **2** at the ground doublet electronic state. Light face numerals: B3-PMP2/6-311++G(3df,2p) calculations with ZPVE corrections. Bold numerals: Effective CCSD(T)/6-311++G(3df,2p) calculations with ZPVE corrections.

Table 3). The TS energies indicate that **3** should dissociate preferentially by direct loss of H-7 rather than undergoing H-atom migration to C-8.

We also investigated in detail the PES region between the valleys for the N-1−H and C-2−H bond dissociations that lead up to **TS1** and **TS9** from **1** and **5**, respectively. The relevant region of PES was mapped by a 15 × 15 point B3LYP/6-31+G(d,p) relaxed scan within the 1.250−1.700 Å interval along the N-1−H and C-2−H coordinates. However, at each point the PES showed negative curvature along either the N-1−H or C-2−H coordinate or both, indicating that there was no first-order saddle point that would interconnect the valleys by a regular transition state. This and the high energy in the relevant PES region (>160 kJ mol^{-1}) strongly indicated that **1** and **5** cannot isomerize by 1,2-hydrogen migration without first dissociating to adenine and an H-atom.

Dissociation Kinetics and Mechanisms. The $^{+}NR^{+}$ mass spectra of $\mathbf{1}^{+}$ and its deuterium-labeled derivatives indicate that loss of H-1 is a major dissociation pathway of the gas-phase radicals. This conclusion is in keeping with the calculated TS energies that show that loss of H-1 through **TS1** is the energetically most favorable dissociation of **1** in its ground doublet electronic state. The $^{+}NR^{+}$ mass spectra also pointed to kinetic isotope effects that affected the abundance ratios of the survivor ions and the adenine cation−radical which was the reionized product of hydrogen loss from **1**. We now use the experimental isotope effects to investigate the internal energy content and distribution in the radicals produced by femtosecond electron transfer. To quantify the neutral dissociations, we presume that the ion fluxes corresponding to $\mathbf{1}^{+}$ and [adenine]$^{+\bullet}$ are proportional to the fluxes of their neutral precursors. This assumption is reasonable because **1** and adenine have similar numbers of atoms and hence very similar ionization cross sections for nonselective collisional ionization.[47] The difference in the collisional ionization cross sections for $C_5H_6N_5$ and $C_5H_5N_5$ is estimated at 100 × (15.53−15.15)/15.15 = 2.5%, which is within the experimental accuracy of the ion intensity measurements. Furthermore, post-reionization dissociations of $\mathbf{1}^{+}$, denoted as [M + H,D], and [adenine]$^{+\bullet}$, denoted as [M], are expected to occur to a similar but small extent, because both ions are substantially stable and their lowest energy dissociations require >350 kJ mol^{-1} threshold energies.[9b,39]

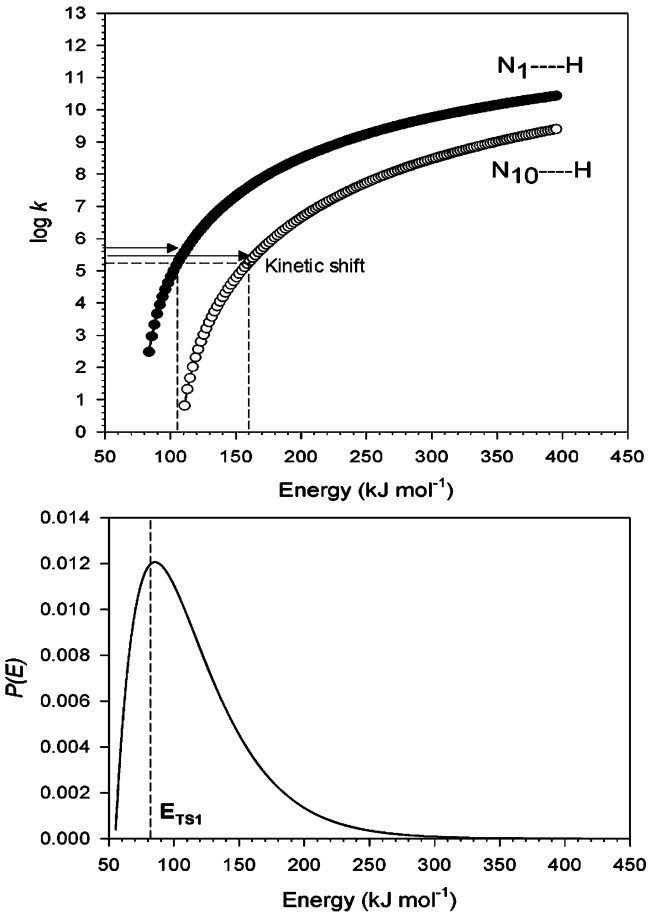

Figure 9. Top panel: RRKM rate constants for N_1−H and N_{10}−H bond dissociations in **1** using B3-PMP2/6-311++G(3df,2p) transition state energies. Bottom panel: Best-fit internal energy distribution function, $P(E)$, for **1** formed by vertical neutralization of thermal $\mathbf{1}^{+}$.

The [M + H,D]/{[M] + [M + H,D]} ratios from the $^{+}NR^{+}$ mass spectra are 0.48, 0.57, and 0.60 for **1**, **1a**, and **1b**, respectively. The ratios are expressed by the kinetic formula for unimolecular dissociation (eq 6), where $k(E)$ is the canonical rate constant, $P(E)$ is the energy deposition function, t is the time for dissociation (5.9 μs for **1**), and E_{TS} is the transition state energy.

$$\frac{[M + H,D]}{\{[M] + [M + H,D]\}} = \int_{E_{TS1}}^{\infty} P(E) e^{-k(E)t}\, dE \qquad (6)$$

The rate constants for the loss of H from **1** and **1a** and the loss of D from **1b** were obtained by RRKM calculations using the B3-PMP2 and effective CCSD(T) TS energies. The RRKM rate constants show that loss of H-1 is 1−2 orders of magnitude faster than loss of H-10 over a >400 kJ mol^{-1} range of internal energies (Figure 9). Both dissociations show substantial kinetic shifts (ΔE_{kin})[48] for dissociations occurring on our experimental time scale, $k = 1/t = 1.66 \times 10^5$ s^{-1}, e.g., $\Delta E_{kin} = 22$ and 50 kJ mol^{-1} for the loss of H-1 and H-10, respectively. To evaluate the integral in eq 6 we used the normalized two-parameter $P(E)$ function (eq 7)[49] that has a maximum at $E_{max} = E_0 + W/2$ and the distribution mean

$$P(E) = \frac{4(E - E_0)}{W^2} e^{-2(E-E_0)/W} \qquad (7)$$

at $\langle E \rangle = E_0 + W$.[49] The best least-squares fit was obtained for $E_0 = 55$ kJ mol^{-1} and $W = 61$ kJ mol^{-1} to give [M + H,D]/

{[M] + [M + H,D]} = 0.49, 0.51, and 0.64 for **1**, **1a**, and **1b**, respectively, when using the RRKM rate constants that were based on B3-PMP2/6-311++G(3df,2p) TS energies. By contrast, the effective CCSD(T)/6-311++G(3df,2p) TS energies appear to be too high for the RRKM rate constants to give a tight fit with the experimental [M + H,D]/{[M] + [M + H,D]} ratios. Hence the B3-PMP2 energies are to be preferred for expressing the dissociation kinetics of **1**, **1a**, and **1b**.

The calculated most probable internal energy in **1**, E_{max} = 55 + 61/2 ≈ 86 kJ mol^{-1}, is close to the sum of the energy acquired by the radical through Franck−Condon effects in vertical electron transfer, E_{FC} = 70 kJ mol^{-1} (Figure 7), and the precursor ion mean rovibrational enthalpy (16 kJ mol^{-1} at 298 K). Note that the precursor ion **1**$^+$ produced by electrospray ionization is thermalized by many collisions with solvent and air molecules at ambient temperature during transfer to the high vacuum region.[41] Hence, the agreement between the internal energy deduced from the RRKM fit (86 kJ mol^{-1}) and that based on the 298 K precursor ion enthalpy and Franck−Condon energy (86 kJ mol^{-1}) appears to be physically sound. The $P(E)$ function (Figure 9) shows that ca. 22% of **1** have internal energies below E_{TS1} and represent inherently stable species. The remaining 26% fraction of nondissociating **1** is due to the 22 kJ mol^{-1} kinetic shift (see above).

The dissociation kinetics of radicals generated by neutralization of precursor ions from gas-phase protonation of adenine are less straightforward to interpret. The $^+NR^+$ spectra show smaller fractions of survivor ions and preferential loss of the hydrogen atom introduced by protonation, e.g., 70% loss of D from **1d**−**3d** and 86% loss of H from **1e**−**3e**. The smaller surviving fraction of adenine radicals in Figures 3 and 4 can be explained by them having higher internal energies than **1** from electrospray/neutralization. The internal energies in **1**−**3** were estimated as described above for **1** with the following differences due to the different ionization mode. The precursor ion internal energy (E_{int}) is composed of the adenine rovibrational enthalpy at the ion source temperature (38 kJ mol^{-1} at 473 K), and a fraction of the energy from exothermic proton transfer. We presume that the excess energy from proton transfer is equipartitioned between the ion (**1**$^+$−**3**$^+$) and the conjugate base of the CI reagent (acetone) in the ratio of their 473 K heat capacities (0.66), which gives E_{int} = 38 + 0.66 × (939−812) = 122 kJ mol^{-1} for **1**$^+$. The precursor ion energies for **2**$^+$ and **3**$^+$ were obtained analogously as 118 and 99 kJ mol^{-1}, respectively. The ion internal energies were combined with the Franck−Condon energies in vertical neutralization of **1**$^+$ (70 kJ mol^{-1}), **2**$^+$ (27 kJ mol^{-1}), and **3**$^+$ (63 kJ mol^{-1}) to give the radical energies as 192, 145, and 162 kJ mol^{-1} for **1**, **2**, and **3**, respectively. These estimates clearly indicate that most of radicals **1**−**3** are formed with internal energies exceeding the respective TS energies for dissociation by loss of H. Moreover, the high internal energies should favor competing dissociations by loss of H from the amino group, and the N-7 → C-8 hydrogen atom migration that would result in loss of H-8. These competing reactions can account for the fractions of H loss other than from N-1, N-3, and N-7 in **1**, **2**, and **3** respectively.

Excited Electronic States. In addition to reionized adenine, the $^+NR^+$ mass spectra of **1**−**3** also show abundant low-mass fragments that arise in part by ring-cleavage dissociations in the radicals. However, the PES for dissociations of **1**−**3** indicate that ring cleavage dissociations are high-energy reactions that should not be competitive with the N−H bond cleavages on the ground doublet electronic states of **1**−**3**. To investigate this issue, we carried out TD-B3LYP/6-311++G(2d,p) calculations

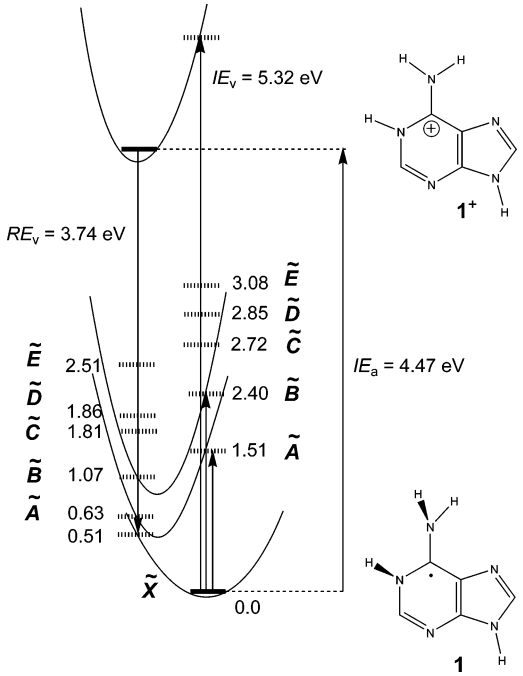

Figure 10. Excited electronic state energies in **1** from TD-B3LYP/6-311++G(2d,p) calculations.

to obtain the excitation energies for the lowest 10 doublet electronic states of **1**−**3**. The first five states for vertical excitation from the relaxed ***X*** state of **1** and for vertically neutralized **1** are shown in Figure 10. The calculations indicate that internal energies needed to drive ring-cleavage dissociations are achieved only in the ***E*** and higher excited states of vertically formed **1** that can further relax nonradiatively to vibrationally superexcited ***X***, ***A***, or ***B*** states. The interesting finding here is that the ***X***−***D*** states of **1** formed directly by vertical electron transfer to **1**$^+$ do not have sufficient energy to cause ring fragmentations. The excitation energies in **2** and **3** follow a very similar trend in that ***E*** and higher excited states are needed to drive ring cleavage dissociations in these radicals, as summarized in Table S18 (Supporting Information).

Hydrogen Atom Additions to Adenine in the Gas Phase and Aqueous Solution. The relative energies for radicals **1**−**3** and **5**−**9** indicate that the C-8 and C-2 adducts are the most stable species in this group of isomers. The question arises as to the reactivity order of the different positions in adenine toward a hydrogen atom attack. We addressed this question by using the transition state theory to calculate bimolecular rate constants for H-atom additions to adenine. The calculations were performed for gas-phase additions including tunnel corrections through the potential energy barriers, as described in the section on Calculations. H-atom additions to all positions in adenine exhibit activation energies, as summarized in Table 4. The activation energies from effective CCSD(T) calculations are uniformly 7.1 ± 1.6 kJ mol^{-1} higher than those from the B3-PMP2 calculations and both sets correlate (slope = 0.941, correlation coefficient, r^2 = 0.977). The thermal rate constants for B3-PMP2 TS energies show dominant addition to C-8 and C-2 over a 200−350 K temperature range. Tunneling through the potential energy barriers has two effects. First, it introduces curvature into the Arrhenius plots (not shown here). Second, it enhances H-atom additions to positions N_3 and N_1 that have somewhat narrower barriers than those for additions to C-8 and C-2. These effects are further visualized by plotting the branching ratios (k_{rel}) with and without inclusion of tunneling effects (Figure 11). In particular, addition to N_3 amounts to

TABLE 4: Transition State Energies and Thermal Rate Constants for H-Atom Additions to Adenine

	B3-PMP2[a]					CCSD(T)[a]			
position	E_{TS}	log k_{298}[b]	k_{rel}	log k'_{298}[c]	k'_{rel}	E_{TS}	log k_{298}[b]	log k'_{298}[c]	k'_{rel}
N_1	35.4	5.72	0.01	6.66	0.03	43.6	4.28	5.23	0.02
C_2	29.2	7.07	0.21	7.52	0.20	37.9	5.55	6.00	0.10
N_3	34.5	6.12	0.02	7.10	0.08	43.8	4.48	5.46	0.03
C_4	52.2	2.85	0.00	3.72	0.00	57.1	2.00	2.86	0.00
C_5	39.0	5.17	0.00	5.82	0.00	44.3	4.24	4.89	0.01
C_6	55.1	2.16	0.00	2.96	0.00	62.6	0.84	1.64	0.00
N_7	39.3	5.02	0.00	6.00	0.01	45.5	3.93	4.91	0.01
C_8	25.4	7.63	0.76	8.04	0.68	31.9	6.50	6.91	0.83

[a] Calculations with the 6-311++G(3df,2p) basis set. [b] Rate constants for H-atom addition (log, mol^{-1} cm^3 s^{-1}) to adenine without including tunnel effects. [c] Rate constants for H-atom addition (log, mol^{-1} cm^3 s^{-1}) to adenine including tunnel effects.

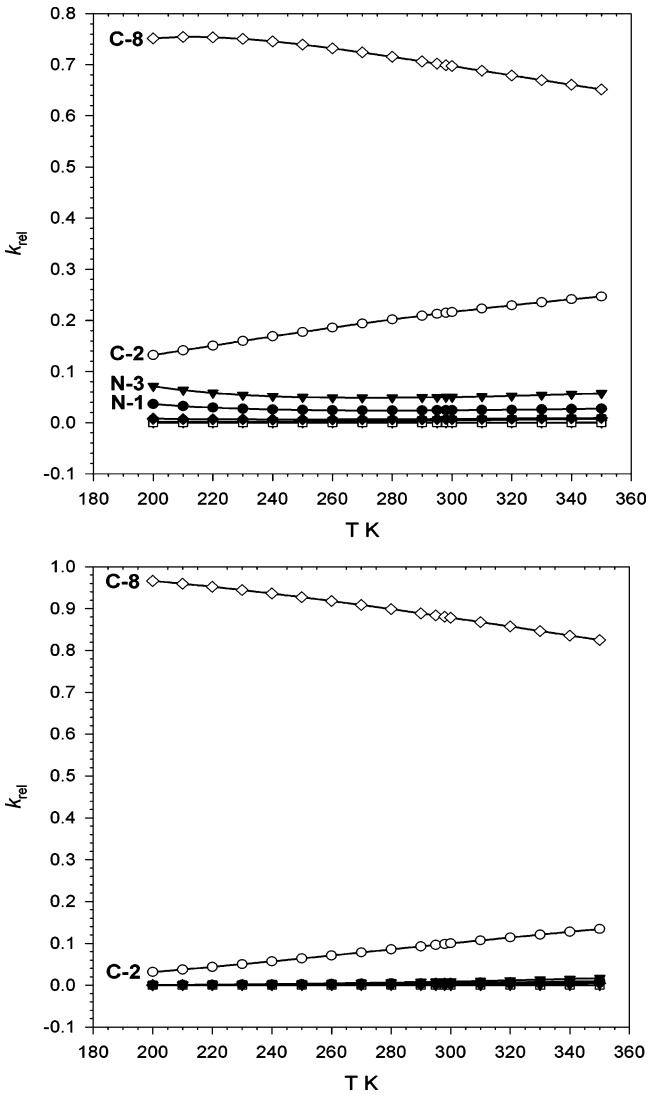

Figure 11. Temperature dependence of relative rate constants for H-atom additions to adenine, $k_{rel,i} = k_i/\sum k_i$: (top) including tunnel effects; (bottom) neglecting tunnel effects.

>10% at 200 K due to tunneling and surpasses addition to C-2 at low temperatures. The tunneling effects are less important at 298 K, where the relative rate constants follow the order of $k_{C-8} > k_{C-2} > k_{N-3} > k_{N-1} > k_{N-7} \cong k_{C-5} > k_{C-4} > k_{C-6}$ regardless of tunneling (Table 4). Note that the transition state energies and relative rate constants for H-atom additions roughly follow the ordering of product stabilities, e.g., **9** > **5** > **1** ≅ **2** ≅ **3** > **7** > **8** ≅ **6**.

To relate the energetics of adenine radicals to their reactivity in solution, we used the Polarizable Continuum Model (PCM)[28] to calculate the relative free energies in a polar dielectric corresponding to an aqueous solution (Table 2). In general, solvation diminishes the energy differences between the tautomeric radicals. The largest changes are found for **1**−**3**, where solvation favors **2** to become the marginally most stable tautomer with the N−H bond. Tautomers **6** and **7** remain high-energy species that are expected not to be significantly populated at equilibrium in solution. The calculated $\Delta G°_{298}$(aq) values are consistent with the reactivity of adenine radicals in solution.[4f] In particular, they show that protonation of adenine anion−radical to give **1** as the initial product must be kinetically controlled, because it does not form the most stable radicals **9** and **5**. However, **1** can exoergically transfer a hydrogen atom to adenine molecules which are present at large excess in solution to form the more stable tautomers **9** and **5**. Although theoretical calculations of hydrogen atom transfer kinetics have not been performed,[50] our present data indicate that at 298 K equilibrium, **9** should be the by far predominating (>99.9%) product.

Conclusions

A combination of electrospray ionization, gas-phase ion chemistry, and collisional electron transfer allowed us to generate the elusive hydrogen atom adduct to N-1 in adenine (**1**), which is thought to be one of the initial intermediates in radiolytic damage of DNA. The radical is an intrinsically stable species in the gas phase and solution. Upon vibrational excitation, it dissociates by expelling the N-1 hydrogen atom to form adenine. Theoretical calculations are in quantitative accord with experiment regarding the properties of **1** and bring further information about the relative stabilities and reactivity of the other hydrogen atom adducts to adenine. The calculated relative free energies of adenine radicals in solution indicate that **1** can react exothermically with adenine to form the more stable C-8 and C-5 adducts, the former of which is predicted to dominate at equilibrium. These computational results support structure assignments from previous pulse radiolysis experiments.

Acknowledgment. Support of this work by the National Science Foundation (grants CHE-0349595 for experiments and CHE-0342956 for computations) is gratefully acknowledged. E.A.S. thanks the Alma and Lloyd West Graduate Student Fellowship for support in the course of this work. P.G. thanks the Fonds National pour la Recherche Scientifique for financial support in the acquisition of the Micromass AutoSpec 6F mass spectrometer and for continuing support. M.T.N. thanks the Department of Chemistry at the University of Washington for warm hospitality and support during his stay in the summer of 2002. The JEOL HX-100 mass spectrometer used in this study was a generous donation from the former Biomembrane Institute, Seattle, WA, courtesy of Professor S. Hakomori.

Supporting Information Available: Tables S1−S17 of B3LYP/6-31+G(d,p) optimized geometries in a Cartesian coordinate format, Table S18 with electronic excitation energies, Figures S1 and S2 with optimized geometries and Figures S3−S9 with potential energy profiles for dissociations. This material is available free of charge via the Internet at http://pubs.acs.org.

References and Notes

(1) Becker, D.; Sevilla, M. D. In *Advances in Radiation Biology. DNA and Chromatin Damage Caused by Radiation*; Lett, J. T., Sinclair, W. K., Eds.; Academic Press: San Diego, CA, 1993; Vol. 17, pp 121−180.

(2) von Sonntag, C. In *Physical and Chemical Mechanisms in Molecular Radiation Biology*; Glass, W. A., Varma, M. N., Eds.; Plenum Press: New York, 1991; pp 287−321.

(3) Chatterjee, A.; Holley, W. R. In *Physical and Chemical Mechanisms in Molecular Radiation Biology*; Glass, W. A., Varma, M. N., Eds.; Plenum Press: New York, 1991; pp 257−285.

(4) (a) Holmes, D. E.; Ingalls, R. B.; Myers, L. S., Jr. *Int. J. Radiat. Biol.* **1967**, *13*, 225−234. (b) Moorthy, P. N.; Hayon, E. *J. Am. Chem. Soc.* **1975**, *97*, 3345−3350. (c) Hissung, A.; von Sonntag, C.; Veltwisch, D.; Asmus, K.-D. *Int. J. Radiat. Biol.* **1981**, *39*, 63−71. (d) Visscher, K. J.; De Haas, M. P.; Loman, H.; Vojnovic, B.; Warman, J. M. *Int. J. Radiat. Biol.* **1987**, *52*, 745−753. (e) Visscher, K. J.; Hom, M.; Loman, H.; Spoelder, H. J. W.; Verberne, J. B. *Radiat. Phys. Chem.* **1988**, *32*, 465−473. (f) Candeias, L. P.; Steenken, S. *J. Phys. Chem.* **1992**, *96*, 937−944. (g) Schaefer, A.; Hüttermann, J.; Kraft, G. *Int. J. Radiat. Biol.* **1993**, *63*, 139−149. (h) Nelson, W. H.; Sagstuen, E.; Hole, E. O.; Close, D. M. *Radiat. Res.* **1992**, *131*, 272−284. For a review see: (i) Steenken, S. *Chem Rev.* **1989**, *89*, 503−520

(5) (a) Zehner, H.; Flossmann, W.; Westhof, E. *Z. Naturforsch.* **1976**, *31C*, 225−231. (b) Zehner, H.; Westhof, E.; Flossmann, W.; Mueller, A. *Z. Naturforsch.* **1977**, *32C*, 1−10. (c) Westhof, E.; Flossmann, W.; Zehner, H.; Mueller, A. *Faraday Discuss. Chem. Soc.* **1977**, *63*, 248−254. (d) Kar, L.; Bernhard, W. A. *Radiat. Res.* **1983**, *93*, 232−253. (e) Close, D. M.; Nelson, W. H. *Radiat. Res.* **1989**, *117*, 367−378.

(6) (a) Sevilla, M. D.; Failor, R.; Clark, C.; Holroud, R. A.; Pettei, M. *J. Phys. Chem.* **1976**, *80*, 353−358. (b) Barnes, J.; Bernhard, W. A. *J. Phys. Chem.* **1993**, *97*, 3401−3408. (c) Barnes, J.; Bernhard, W. A. *J. Phys. Chem.* **1994**, *98*, 10969−10977.

(7) (a) Nguyen, V. Q.; Tureček, F. *J. Mass Spectrom.* **1996**, *31*, 1173−1184. (b) Nguyen, V. Q.; Tureček, F. *J. Mass Spectrom.* **1997**, *32*, 55−63. (c) Nguyen, V. Q.; Tureček, .F *J. Am. Chem. Soc.* **1997**, *119*, 2280−2290. (d) Tureček, F. *J. Mass Spectrom.* **1998**, *33*, 779−795. (e) Wolken, J. K.; Tureček, F. *J. Phys. Chem. A* **1999**, *103*, 1905−1912. (f) Wolken, J. K.; Tureček, F. *J. Am. Chem. Soc.* **1999**. *121*, 6010−6018. (g) Wolken, J. K.; Tureček, F. *J. Phys. Chem. A* **1999**, *103*, 6268−6281.

(8) (a) Wolken, J. K.; Syrstad, E. A.; Vivekananda, S.; Tureček, F. *J. Am. Chem. Soc.* **2001**, *123*, 5804−5805. (b) Syrstad, E. A.; Vivekananda, S.; Tureček, F. *J. Phys. Chem. A* **2001**, *105*, 8339−8351. (c) Wolken, J. K.; Tureček, F. *J. Phys. Chem. A* **2001**, *105*, 8352−8360.

(9) (a) Wolken, J. K.; Tureček, F. *J. Am. Soc. Mass Spectrom.* **2000** *11*, 1065−1071. (b) Chen, X.; Syrstad, E. A.; Nguyen, M. T.; Gerbaux, P.; Tureček, F. *J. Phys. Chem. A* **2004**, *108*, 9283−9293.

(10) (a) Curtis, P. M.; Williams, B. W.; Porter, R. F. *Chem. Phys. Lett.* **1979**, *65*, 296−299. (b) Burgers, P. C.; Holmes, J. L.; Mommers, A. A.; Terlouw, J. K. *Chem. Phys. Lett.* **1983**, *102*, 1−3. (c) Danis, P. O.; Wesdemiotis, C.; McLafferty, F. W. *J. Am. Chem. Soc.* **1983**, *105*, 7454−7456. For most recent reviews see: (d) Zagorevskii, D. V. In *Comprehensive Coordination Chemistry II*; McCleverty, J. A., Meyer, T. J., Eds.; Elsevier: Oxford, UK, 2004; pp 381−386. (e) Tureček, F. *Top. Curr. Chem.* **2003**, *225*, 77−129. (f) Tureček, F. In *Encyclopedia of Mass Spectrometry*; Armentrout, P. B., Ed.; Elsevier: Amsterdam, The Netherlands, 2003; Vol. 1, Chapter 7, pp 528−541. (g) Zagorevskii, D. V. *Coord. Chem. Rev.* **2002**, *225*, 5−34. (h) Gerbaux, P.; Wentrup, C.; Flammang, R. *Mass Spectrom. Rev.* **2000**, *19*, 367−389. (i) Zagorevskii, D. V.; Holmes, J. L. *Mass Spectrom. Rev.* **1999**, *18*, 87−118. (j) Schalley, C.; Hornung, G.; Schröder, D.; Schwarz, H. *Chem. Soc. Rev.* **1998**, *27*, 91−104.

(11) (a) Sadílek, M.; Tureček, F. *J. Phys. Chem.* **1996**, *100*, 9610−9614. (b) Sadílek, M.; Tureček, F. *Chem. Phys. Lett.* **1996**, *263*, 203−208. (c) Polášek, M.; Tureček, F. *J. Phys. Chem. A* **2001**, *105*, 1371−1382.

(12) (a) Kuhns, D. W.; Tran, T. B.; Shaffer, S. A.; Tureček, F. *J. Phys. Chem.* **1994**, *98*, 4845−4853. (b) Kuhns, D. W.; Tureček, F. *Org. Mass Spectrom.* **1994**, *29*, 463−469. (c) Sadílek, M.; Tureček, F. *J. Phys. Chem.* **1996**, *100*, 224−232.

(13) Laxer, A.; Major, D. T.; Gottlieb, H. E.; Fischer, B. *J. Org. Chem.* **2001**, *66*, 5463−5481.

(14) (a) Tureček, F.; Gu, M.; Shaffer, S. A. *J. Am. Soc. Mass Spectrom.* **1992**, *3*, 493−501. (b) Tureček, F. *Org. Mass Spectrom.* **1992**, *27*, 1087−1097.

(15) Seymour, J. L.; Syrstad, E. A.; Langley, C. C.; Tureček, F. *Int. J. Mass Spectrom.* **2003**, *228*, 687−702.

(16) Shaffer, S. A.; Tang, K.; Anderson, G. A.; Prior, D. C.; Udseth, H. R.; Smith, R. D. *Rapid Commun. Mass Spectrom.* **1997**, *11*, 1813−1817.

(17) Bateman, R. H.; Brown, J.; Lefevere, M.; Flammang, R.; Van Haverbeke, Y. *Int. J. Mass Spectrom Ion Processes* **1992**, *115*, 205−218.

(18) (a) Frisch, M. J.; Trucks, G. W.; Schlegel, H. B.; Scuseria, G. E.; Robb, M. A.; Cheeseman, J. R.; Zakrzewski, V. G.; Montgomery, J. A.; Stratmann, R. E.; Burant, J. C.; Dapprich, S.; Millam, J. M.; Daniels, A. D.; Kudin, K. N.; Strain, M. C.; Farkas, O.; Tomasi, J.; Barone, V.; Cossi, M.; Cammi, R.; Mennucci, B.; Pomelli, C.; Adamo, C.; Clifford, S.; Ochterski, J.; Petersson, G. A.; Ayala, P. Y.; Cui, Q.; Morokuma, K.; Malick, D. K.; Rabuck, A. D.; Raghavachari, K.; Foresman, J. B.; Cioslowski, J.; Ortiz, J. V.; Stefanov, B. B.; Liu, G.; Liashenko, A.; Piskorz, P.; Komaromi, I.; Gomperts, R.; Martin, R. L.; Fox, D. J.; Keith, T.; Al-Laham, M. A.; Peng, C. Y.; Nanayakkara, A.; Gonzalez, C.; Challacombe, M.; Gill, P. M. W.; Johnson, B. G.; Chen, W.; Wong, M. W.; Andres, J. L.; Head-Gordon, M.; Replogle, E. S.; Pople, J. A. *Gaussian 98*; Revision A.6; Gaussian, Inc.: Pittsburgh, PA, 1998. (b) Frisch, M. J.; Trucks, G. W.; Schlegel, H. B.; Scuseria, G. E.; Robb, M. A.; Cheeseman, J. R.; Montgomery, J. A., Jr.; Vreven, T.; Kudin, K. N.; Burant, J. C.; Millam, J. M.; Iyengar, S. S.; Tomasi, J.; Barone, V.; Mennucci, B.; Cossi, M.; Scalmani, G.; Rega, N.; Petersson, G. A.; Nakatsuji, H.; Hada, M.; Ehara, M.; Toyota, K.; Fukuda, R.; Hasegawa, J.; Ishida, M.; Nakajima, T.; Honda, Y.; Kitao, O.; Nakai, H.; Klene, M.; Li, X.; Knox, J. E.; Hratchian, H. P.; Cross, J. B.; Adamo, C.; Jaramillo, J.; Gomperts, R.; Stratmann, R. E.; Yazyev, O.; Austn, A. J.; Cammi, R.; Pomelli, C.; Ochterski, J. W.; Ayala, P. Y.; Morokuma, K.; Voth, G. A.; Salvador, P.; Dannenberg, J. J.; Zakrzewski, V. G.; Dapprich, S.; Daniels, A. D.; Strain, M. C.; Farkas, O.; Malick, D. K.; Rabuck, A. D.; Raghavachari, K.; Foresman, J. B.; Ortiz, J. V.; Cui, Q.; Baboul, A. G.; Clifford, S.; Cioslowski, J.; Stefanov, B. B.; Liu, G.; Liashenko, A.; Piskorz, P.; Komaromi, I.; Martin, R. L.; Fox, D. J.; Keith, T.; Al-Laham, M. A.; Peng, C. Y.; Nanayakkara, A.; Challacombe, M.; Gill, P. M. W.; Johnson, B.; Chen, W.; Wong, M. W.; Gonzalez, C.; Pople, J. A. *Gaussian 03*, Revision B.05; Gaussian, Inc.: Pittsburgh, PA, 2003.

(19) (a) Becke, A. D. *J. Chem. Phys.* **1993**, *98*, 1372−1377. (b) Becke, A. D. *J. Chem. Phys.* **1993**, *98*, 5648−5652. (c) Stephens, P. J.; Devlin, F. J.; Chabalowski, C. F.; Frisch, M. J. *J. Phys. Chem.* **1994**, *98*, 11623−11627.

(20) (a) Schlegel, H. B. *J. Chem. Phys.* **1986**, *84*, 4530−4534. (b) Mayer, I. *Adv. Quantum Chem.* **1980**, *12*, 189−262.

(21) Tureček, F. *J. Phys. Chem. A* **1998**, *102*, 4703−4713.

(22) (a) Tureček, F.; Carpenter, F. H.; Polce, M. J.; Wesdemiotis, C. *J. Am. Chem. Soc.* **1999**, *121*, 7955−7956. (b) Tureček, F.; Polášek, M.; Frank, A. J.; Sadílek. M. *J. Am. Chem. Soc.* **2000**, *122*, 2361−2370. (c) Polášek, M.; Tureček, F. *J. Am. Chem. Soc.* **2000**, *122*, 9511−9524. (d) Tureček, F.; Syrstad, E. A. *J. Am. Chem. Soc*. **2003**, *125*, 3353−3369. (e) Tureček, F.; Yao, C. *J. Phys. Chem. A* **2003**, *107*, 9221−9231.

(23) (a) Rablen, P. R.; Bentrup, K. H. *J. Am. Chem. Soc.* **2003**, *125*, 2142−2147. (b) Rablen, P. R. *J. Org. Chem.* **2000**, *65*, 7930−7937. (c) Rablen, P. R. *J. Am. Chem. Soc.* **2000**, *122*, 357−368. (d) Hirama, M.; Tokosumi, T.; Ishida, T.; Aihara, J. *Chem. Phys.* **2004**, *305*, 307−316.

(24) Čížek, J.; Paldus, J.; Šroubková, L. *Int. J. Quantum Chem.* **1969**, *3*, 149−167.

(25) Purvis, G. D.; Bartlett, R. J. *J. Chem. Phys.* **1982**, *76*, 1910−1918.

(26) Curtiss, L. A.; Raghavachari, K.; Pople, J. A. *J. Chem. Phys.* **1993**, *98*, 1293−1298.

(27) Stratmann, R. E.; Scuseria, G. E.; Frisch, M. J. *J. Chem. Phys.* **1998**, *109*, 8218−8224.

(28) (a) Barone, V.; Cossi, M.; Tomasi, J. *J. Chem. Phys.* **1997**, *107*, 3210−3221. (b) Cossi, M.; Scalmani, G.; Rega, N.; Barone, V. *J. Chem. Phys.* **2002**, *117*, 43−54.

(29) Zhu, L.; Hase, W. L. *Quantum Chemistry Program Exchange*; Indiana University: Bloomington, IN, 1994; Program No. QCPE 644.

(30) Frank, A. J.; Sadílek, M.; Ferrier, J. G.; Tureček, F. *J. Am. Chem. Soc.* **1997**, *119*, 12343−12353.

(31) Gilbert, R. G.; Smith, S. C. *Theory of Unimolecular and Recombination Reactions*; Blackwell Scientific Publications: Oxford, UK, 1990; pp 52−132.

(32) Tureček, F.; Syrstad, E. A. *J. Am. Chem. Soc*. **2003**, *125*, 3353−3369.

(33) (a) Syrstad, E. A.; Stephens, D. D.; Tureček, F. *J. Phys. Chem. A* **2003**, *107*, 115−126. (b) Chen, X.; Syrstad, E. A.; Tureček, F. *J. Phys. Chem. A* **2004**, *108*, 4163−4173.

(34) Truhlar, D. G.; Kuppermann, A. *J. Am. Chem. Soc.* **1971**, *93*, 1840−1851.

(35) Eckart, C. *Phys. Rev.* **1930**, *35*, 1303−1309.

(36) Bell, R. P. *The Tunnel Effect in Chemistry*; Chapman and Hall: London, UK, 1980; p 27.

(37) Major, D. T.; Laxer, A.; Fischer, B. *J. Org. Chem.* **2002**, *67*, 790−802.

(38) Christensen, J. J.; Rytting, J. H.; Izatt, R. M. *Biochemistry* **1970**, *9*, 4907−4913.

(39) Tureček, F.; Chen, X. *J. Am. Soc. Mass Spectrom.* **2005**, *16*, 1713−1726.

(40) (a) Gatlin, C. L.; Tureček, F. *Anal. Chem.* **1994**, *66*, 712−718. For a review, see: (b) Van Berkel, G. J. In *Electrospray Ionization Mass Spectrometry*; Cole, R. B., Ed.; John Wiley & Sons: New York, 1997; Chapter 2, pp 65−106.

(41) (a) Drahos, L.; Heeren, R. M. A.; Collette, C.; De Pauw, E.; Vekey, K. *J. Mass Spectrom.* **1999**, *34*, 1373−1379. (b) Naban-Maillet, J.; Lesage, D.; Bossee, A.; Gimbert, Y.; Sztaray, J.; Vekey, K. *J. Mass Spectrom.* **2005**, *40*, 1−8.

(42) Nelson, C. C.; McCloskey, J. A. *J. Am. Chem. Soc.* **1992**, *114*, 3661−3668.

(43) From the corresponding proton affinities (kJ mol^{-1}) of water (691) and methanol (754). NIST Standard Reference Database Number 69, March, 2003 Release: http://webbook.nist.gov/chemistry

(44) Harrison, A. G. *Chemical Ionization mass Spectrometry*, 2nd ed.; CRC Press: Boca Raton, FL, 1992; p 30.

(45) See the NIST database (ref 43) for the reference electron−ionization mass spectrum of adenine.

(46) (a) Reynisson, J.; Steenken, S. *Phys. Chem. Chem. Phys.* **2005**, *7*, 659−665. (b) Wetmore, S. D.; Boyd, R. J.; Eriksson, L. A. *J. Phys. Chem. B* **1998**, *102*, 10602−10614.

(47) Fitch, W. L.; Sauter, A. D. *Anal. Chem.* **1983**, *55*, 832−835.

(48) Lifshitz, C. *Mass Spectrom. Rev.* **1982**, *1*, 309−348.

(49) (a) Gerbaux, P.; Tureček, F. *J. Phys. Chem. A* **2002**, *106*, 5938−5950. (b) Tureček, F. *Int. J. Mass Spectrom.* **2003**, *227*, 327−338.

(50) Calculations of reliable transition state energies for H-atom transfer between **1** and adenine would require a high-level theory that is beyond our present computational capabilities.